

## La-DOPED ZNO THIN FILMS PREPARED BY SPRAY PYROLYSIS WITH MOVING NOZZLE: STUDY OF PHYSICAL PROPERTIES AND ADSORPTION ABILITY OF THE COPPER

M. T. TLIBA<sup>a,b\*</sup>, A. BENHAOUA<sup>a</sup>, R. GHERIANI<sup>a,b</sup>, B. BENHAOUA<sup>a,c</sup>,  
A. RAHAL<sup>a</sup>, C. BOUKAOUS<sup>a,d</sup>, A. TLIBA<sup>a</sup>

<sup>a</sup>Lab. VTRS, Faculty of Science & Technology, Univ. El-Oued, El Oued 39000, Algeria

<sup>b</sup>Faculty of Mathematics and Material Sciences, Univ. Ouargla, Ouargla 30000, Algeria

<sup>c</sup>Renewable Energy Development Unit in Arid Zones (REDUAZ), Univ. El-Oued, El Oued 39000, Algeria

<sup>d</sup>Lab. Microstructures and Defects in Materials, Univ. Constantine 25000, Algeria

0-5wt.% Lanthanum doped zinc oxide thin films were elaborated by spray pyrolysis technique, with moving nozzle, on 375°C heated glass. Zinc acetate and Lanthanum chloride are used as sources precursor of ZnO and La doping, respectively. Effect of lightly 0-5wt.% La amount concentration on optical, structural, topographical properties of La-doped ZnO thin films and their adsorptive ability on the copper ions from water, were investigated. In the visible range, the transmittance of all samples is greater than 75% and increases after La doping. Optical gap was found to be in 3.26-3.28eV scale. X-ray diffraction showed that the thin films have hexagonal wurtzite structure with a strong (002) as preferred orientation, whereas the crystalline size was ranged in 17.23-37.41nm. An enhancement in the removal of the ion copper from water solution was observed after La doping. As a result Lanthanum is a good quality doping element for increasing the adsorptive ability of ZnO thin films by augmenting its active surface area or by intensifying the permanent polarity along *c* direction.

(Received July 22, 2018; Accepted October 18, 2018)

**Keywords:** Spray pyrolysis, thin films, La doped ZnO, X-ray diffraction, heavy metal

### 1. Introduction

As driven from semiconductor material, ZnO is considered as transparent conducting oxides. At room temperature, it has a wide band gap (3.3eV) and high exciton binding energy (60 meV) [1, 2]. It is one of the common materials used in microelectronic devices and many applications, such as light-emitting diodes, solar cells, transparent conducting contacts, liquid crystal displays, field-effect transistors, photocatalyst and gas sensors devices [3-8]. ZnO thin films can be produced by several methods. Many workers have shown that physical properties such as optical parameters, structural and morphological properties of ZnO may be modified by the used techniques. Based on its simplicity, safety, and inexpensive equipment the famous spray pyrolysis is one of the more used methods due to its feasible wide area depositions with low temperature and easy control of film thickness [9], yet using such technique with continuous drop of solution on substrate, may provoke temperature fall of the substrates and limit solvent evaporation. At my best knowledge, classical spray pyrolysis needs interruptions (spending time) of solution flux to keep constant the substrate temperature [10]. This technique needs to be ameliorated under the optic of maintaining substrate temperature constant.

Trivalent rare earth such as La-doped ZnO evokes few concentrations of researchers. Structure and optical properties of La-doped ZnO nanorods, at a doping level of 0.2, 0.5, and 1.0

\*Corresponding author: meriemtouati39@gmail.com

mol.% La-ZnO were briefly studied in literature [11] and recently some physical investigations, on 0-4wt.% La-doped ZnO nanorods were done [12]. Because copper is considered as heavy metals which constitute dangerous problems for our environment, namely water life, and people health. Lately, for wastewater treatment, it was found that ZnO thin films are more effective and best adsorbents for taking away copper ions from wastewater [13-15].

Based on the above reasons, the goal of this work is to focus more, firstly on spray pyrolysis technique with moving nozzle as originality to maintain constant the heat of the substrates and leads to rapid solvent evaporation hence nozzle motion leads to small area temperature fall, secondly to investigate the effect of lightly La doping average stepped as (0, 1, 2, 3 and 5wt.%) on optical, structural and surface morphological properties of ZnO thin films deposited on 375°C heated glass substrate. Lastly, the effect of the 0-5wt. % La-doped ZnO, on the copper adsorption, as an application in removing ions copper from  $1.2 \cdot 10^{-2}$  molar  $\text{CuCl}_2$  synthetic solution, will be undergone in this proposed study.

## 2. Experimental details

### 2.1. Films preparation

By dissolving (0.5M) zinc acetate dihydrate ( $\text{Zn}(\text{CH}_3\text{COO})_2 \cdot 2\text{H}_2\text{O}$ ) in the solvent containing equal volumes (ratio 1/2:1/2) of double distilled water and absolute methanol solution (purity: 99.995%), undoped ZnO thin films solution was ready. Few drops (drop by drop) of concentrated acetic acid solution were added to the prepared solution as a stabilizer. The mixture solution was stirred at 50°C for 90 min to have a clear and transparent solution. For Lanthanum doping, Lanthanum chloride heptahydrate ( $\text{LaCl}_3 \cdot 7\text{H}_2\text{O}$ ) with appropriated ratio of La/Zn (0, 1, 2, 3 and 5wt. %) was added to the precedent solution. Each solution, with appropriated ratio of La/Zn, became homogeneous and clear after stirring for 90 min at 55°C too. For non-doped and La-doped ZnO thin films, the resulting solutions were sprayed, via moving nozzle, on 375°C heated glass substrates. The moving nozzle was used to preserve constant the heat of the substrates and evaporate rapidly the solvent leading to homogeneous thin films. The deposition of ZnO thin films was performed for 12 min with keeping the moving nozzle-substrate distance equal to 5cm. The substrates are microscope glass (ref: R217102) cleaned with alcohol in ultrasonically bath and blow-dried with compressed air.

### 2.2. Preparation of heavy-metal ions solution

To investigate the capacities of the as prepared undoped and La-doped ZnO thin films in removing heavy metal ions ( $\text{Cu}^{+2}$ ), sheets having as surface ( $2.5 \times 3.5 \text{cm}^2$ ) and 1.6 mg as weight of product of La-doped and undoped ZnO were introduced into 40mL of wastewater solution containing  $1.2 \cdot 10^{-2} \text{M}$   $\text{Cu}^{+2}$  obtained by dissolving 0.085g of  $\text{CuCl}_2$  in 40ml of double distilled water. The as obtained mixed system was let for 30-60min to ensure sufficient interaction between sheets of films, as adsorbents, and heavy-metal ions ( $\text{Cu}^{2+}$ ). Cyclic voltammetric apparatus (Volta Lab PGZ 301) with conventional three electrodes cell was used to analyze the concentration of heavy metal ions before and after adsorption. As a counter electrode (CE: anode), a platinum plate was used, whereas for a working (WE) and a reference electrode (RE) we have used a graphite carbon and saturated KCl electrode (SCE), respectively. The removal percentage of the  $\text{Cu}^{+2}$  ions was obtained using the following equation:

$$R = \left( \frac{C_0 - C_e}{C_0} \right) \times 100\% \quad (1)$$

where  $C_0$ ,  $C_e$  is the initial concentration at  $t=0$  min and the final concentration of ions copper in solution after 60 min respectively. To know the effect of La-doped ZnO on the copper adsorption from wastewater, a series of synthetic ion copper solution, at the concentration of  $1.2 \cdot 10^{-2} \text{M}$ , was prepared by dissolving 0.085g of  $\text{CuCl}_2$  in 40ml of double distilled water. The sheets having surface ( $A_{\text{ZnO}}=2.5 \times 3.5 \text{cm}^2$ ) and have 1.6 mg as weight of product ( $\rho_{\text{ZnO}} \times \text{volume}_{\text{ZnO}}=$

$\rho_{\text{ZnO}} \times A_{\text{ZnO}} \times t$ ), of 0-5 wt.% La doped ZnO thin films were separately introduced in the series of the synthetic solutions. Each sheet was immersed for 60 min then it dipped out from the solution. At room temperature (rt), all measurements were carried out.

### 2.3. Characterization techniques

Optical transmittance spectra were carried out using a UV-Visible spectrophotometer (Shimadzu, Model 1800) operating in the range of 300-900nm. Structural analysis of the samples was done using X-ray diffraction (XRD, Bruker AXS type 8D operating under an X-ray source at 40 KV and 30 mA condition with Cu K $\alpha$  radiation ( $\lambda=1.5406\text{\AA}$ ) and the  $2\theta$  value was swapped between  $30^\circ$  and  $55^\circ$ . Surface morphology of the samples was survived using a scanning electron microscope (SEM: TESCAN VEGA TS 5130 MM), whereas film thickness was optically estimated to be ( $t \approx 323\text{nm}$ ) in respect to Swanepoel law.

## 3. Results and discussion

### 3.1. Optical properties

Fig.1 displays UV-visible (300-900 nm) transmittance spectra of 0-5wt. % La doped ZnO thin films. As seen in the wavelength range 400-900 nm, spectra of all films exhibit high transmittance values of about 75-92% indicating a better quality of transparency layers. It is easily seen from Fig. 1 that transmittance of the films increases with La doping level when compared to undoped one. This may be due to the broadening of the optical band gap as carried out in the literature [16]. The transmittance average of the films, before and after doping, is shown in Table 1. For all the films, in the region between 370-400nm, the transmittance decreased abruptly due to the fundamental absorption edge attributed to the transition between the valence band and conduction one. This edge is used to calculate the gap  $E_g$  of the films.  $E_g$  values were deduced from transmission measurements with the help of Tauc's relation [17]:

$$(\alpha h\nu)^2 = B(h\nu - E_g) \quad (2)$$

where  $h\nu$  and  $E_g$  are the photon energy and the band gap energy of the semiconductor; whereas  $B$  is a constant. As seen in Fig.2 a typical variation of  $(\alpha h\nu)^2$  upon photon energy ( $h\nu$ ) was used for determining optical band gap ( $E_g$ ) of undoped ZnO as an example. For all thin films,  $E_g$  is deduced by extrapolation from the linear region to  $(\alpha h\nu)^2=0$ , in the range between 370 and 400nm (3.26-3.28 eV). Deducted values of the optical band gap  $E_g$  are shown in Table1. Moreover to carry out information about the disorder in the film network, Urbach energy ( $E_u$ ), which is directly associated to the later was used as follow [18]:

$$\alpha = \alpha_0 \exp(h\nu/E_u) \quad (3)$$

where  $\alpha$  is the absorption coefficient,  $h\nu$  and  $E_u$  are photon energy and Urbach energy respectively; whereas  $\alpha_0$  is constant. The drawn of  $\ln\alpha$  upon the photon energy ( $h\nu$ ) was used in deducing Urbach energy as it was shown in the inset of Fig. 2.  $E_u$  values were obtained from the inverse of the slope of  $\ln\alpha$  versus ( $h\nu$ ).  $E_u$  and  $E_g$  are reported in Table 1.

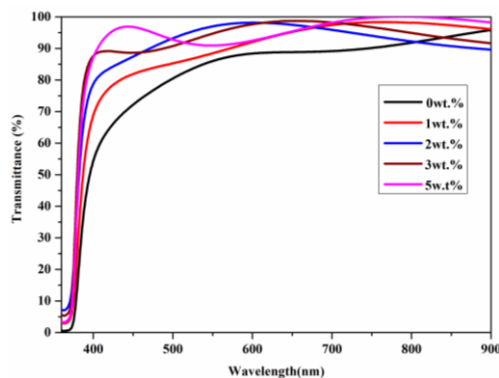


Fig.1. Transmissions spectra of 0-5 wt. % La doped ZnO thin films elaborated by spray pyrolysis with moving nozzle versus wavelength at fixed time deposition (12min).

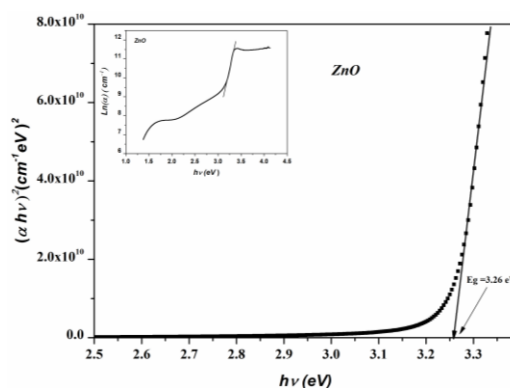


Fig.2.  $(\alpha hv)^2$  plot versus photon energy of undoped ZnO thin film. The inset shows the drawn of  $\ln \alpha$  as a function of photon energy ( $h\nu$ ) to deduce the Urbach energy.

Table 1. Optical parameters of 0-5 wt. % La doped ZnO thin films: Optical transmittance T, band gap energy  $E_g$  and Urbach energy  $E_u$ .

La/Zn (wt. %)	T(%)	$E_g$ (eV)	$E_u$ (meV)
0.00	75.92	3.268	84.85
1.00	82.80	3.269	84.00
2.00	84.69	3.273	75.02
3.00	89.66	3.280	52.02
5.00	92.97	3.277	65.60

Shown in Fig. 3 are the variations of the optical gap together with the Urbach tail energy as a function of La concentration. The slight increase in optical band gap can be explained in terms of Burstein-Moss band gap widening [19] or may be due to the rearrangement of the atoms in the crystalline lattice which decreases defects in the microstructure. Also, it can be seen that a minimum Urbach energy was reached with 3wt.% La-doped ZnO thin films crediting to the decrease of defects [20].

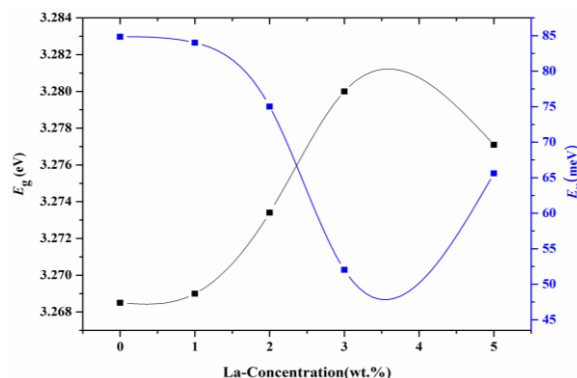


Fig.3. Optical band  $E_g$  and Urbach energy  $E_u$  variations of 0-5 wt. % La doped ZnO thin films.

## 3.2. Structural properties

### 3.2.1. X-ray diffraction

XRD patterns of 0-5wt. % La-doped ZnO thin films are shown in Fig. 4. All the obtained spectra of the films much well with the space group P63mc (186) owing JCPDS card No36-1451 of the hexagonal wurtzite ZnO structure[21]. As can be seen, all films exhibit a low surface free energy growth along (002) peak plane of ZnO which so called  $c$ -axis orientation as reported in the literature [22-24]. Furthermore, this significant (002) diffraction peak increases with increasing the La doping concentration until 3 wt.%, in comparison with the undoped one leading to announce the crystallinity enhancement of the films. In the inset of Fig. 4 displays the XRD patterns ranged in  $(34-35^\circ.40)$ . It was noted that a diffraction peak along (002) plane exhibits small shift to lower angles when La doping is lower than 3wt.% range of La/Zn in the solution compared to the non-doped one. As registered maximum shift value was  $(0.1^\circ)$  with 5wt. % La doping. This shift may be due to the incorporated  $\text{La}^{3+}$  ions in the ZnO matrix by substituting  $\text{Zn}^{2+}$  ones, hence there is a great difference in ion radius between  $\text{Zn}^{2+}$  ( $0.74 \text{ \AA}$ ) and  $\text{La}^{3+}$  ( $1.15 \text{ \AA}$ ) leading to an increase in parameters lattice as it will be discussed bellow. A return toward initial angles value was remarked when La doping reach 3wt. % (see inset of Fig.4) which means that  $\text{La}^{3+}$  ions losses its substitution position. As consequence, from this loss, a decrease in parameters lattice has been expected and well observed (see for instance Fig.5).

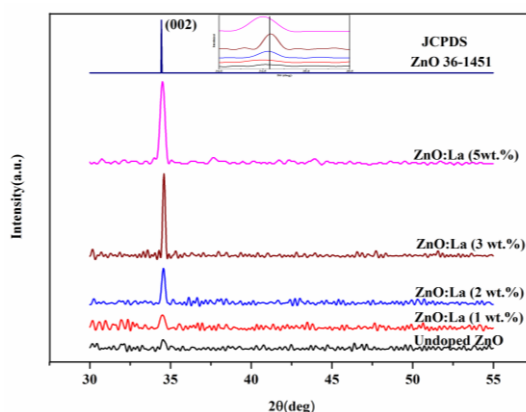


Fig.4. X-ray diffraction patterns of ZnO films, elaborated by spray pyrolysis with moving nozzle as a function of La-concentration.

The average size of the crystallites ( $G$ ) of all the samples along the  $c$ -axis (002) can be calculated using the Debye-Scherer's equation [25]:

$$G = \frac{0.9\lambda}{\beta \cos \theta} \quad (4)$$

where  $\lambda$  is the wavelength of X-ray ( $\lambda=0.15406$ ),  $\beta$  and  $\theta$  are the full width at half maximum (*FWHM*) of (002) diffraction peaks and the Bragg angle, respectively.

For the calculation of lattice parameter  $c$  and the inter-planer spacing  $d_{hkl}$ , we have used the following formulas [26]:

$$2d_{hkl} \sin \theta = n\lambda \quad (5)$$

and

$$\frac{1}{d_{hkl}^2} = \frac{4}{3} \left( \frac{h^2 + hk + k^2}{a^2} \right) + \frac{l^2}{c^2} \quad (6)$$

where  $n$  is the order of diffraction,  $d_{hkl}$  is the plane spacing and  $\theta$  is the diffraction angle,  $a$  and  $c$  are the lattice parameters, whereas  $hkl$  are the Miller planes indices.

The crystallite size ( $G$ ),  $d_{hkl}$ ,  $\theta$  and  $c$  values are illustrated in Table 2. It was found that  $c$  values, for undoped and La-doped, are lower than the standard values given in JCPDS file (No.36-1451) where ( $c_0= 0.5206$  nm).

Table 2. Recapitulating measured values of 0-5 wt. % La doped ZnO thin films: Bragg angle ( $2\theta$ ), inter planar spacing ( $d$ ), crystallite size ( $G$ ) and lattice parameter  $c$ .

La/Zn(wt.%)	$hkl$	$2\theta(\text{deg})$	$d_{hkl}(\text{\AA})$	$G(\text{nm})$	$c(\text{nm})$
0.00	(002)	34.5734	2.5935	18.65	0.5187
1.00	(002)	34.5002	2.5988	17.23	0.5197
2.00	(002)	34.5601	2.5945	30.69	0.5189
3.00	(002)	34.5940	2.5920	37.41	0.5184
5.00	(002)	34.5125	2.5979	21.51	0.5195

The  $G$  and  $c$  variation with La-concentration are shown in Fig. 5. As it was observed, a slight decrease in the crystallite size until 1wt % of doping. Beyond this level, monotonically increase with increasing La doping, to arrive at a maximum value (37.41nm) with 3wt.% La doping was observed. This increase in crystallite size  $G$  reveals the enhancement of the crystallinity growth along the (002) plane of La-doped ZnO thin film. The same results were remarked in the literature [20, 27]. The lattice parameter  $c$  increases to reach a maximum value at 1wt.% La doping, after this it decreases, with La doping increase, to attain minimum value at 3wt.% La doping and then increases beyond. The increase in lattice parameter  $c$  of La-doped ZnO may be due to the large difference between the substitute ionic radius of  $\text{La}^{3+}$  (1.15 Å) with  $\text{Zn}^{2+}$  (0.74 Å) into the ZnO lattice and its decrease may be attributed to the loss in the substitutional position of  $\text{La}^{3+}$  ion in the ZnO lattice.

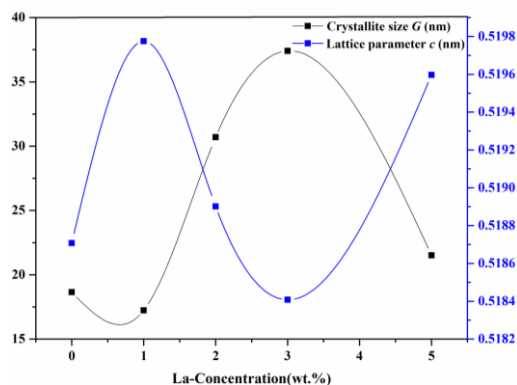


Fig.5. Crystallite size  $G$  and lattice parameter  $c$ , variations of 0-5 wt. % La doped ZnO thin films elaborated by spray pyrolysis with moving nozzle.

### 3.2.2. Scanning electron microscopy

The surface morphology of 0-5 wt. % La-doped ZnO thin films as a function of La concentration is shown in Fig. 6. At the same SEM magnification Fig. 6a-d show SEM images of undoped, 1, 3 and 5 wt.% La doped ZnO thin films, respectively. As clearly seen, the whole samples have a homogenous distribution of ZnO product on the substrates revealing the feasibility of the moving nozzle. The morphology of ZnO films was remarkably changed with La doping. For non-doped ZnO thin film, grains with little dimension, randomly distributed takes place. For 1 and 3 wt. % La doped thin films the grains growth takes a perpendicular and regular direction to the substrate with very smaller grains size. This regular direction was carried out by XRD patterns, whereas the 5 wt. % La doped thin film reveals an increase in the crystallite size. It is worth noting that the decrease in grain size provides the samples great surface area. As clearly seen in Fig. 6 b-c, numerous pores are present on the surface of the samples which participates also in the increase of the surface area. The pores presence on the surface may be resulting from evaporation of the organic solvent [16], or it may be also due to nucleation and coalescence process of crystallite growth during the deposition of La-doped ZnO as carried out in the literature [28].

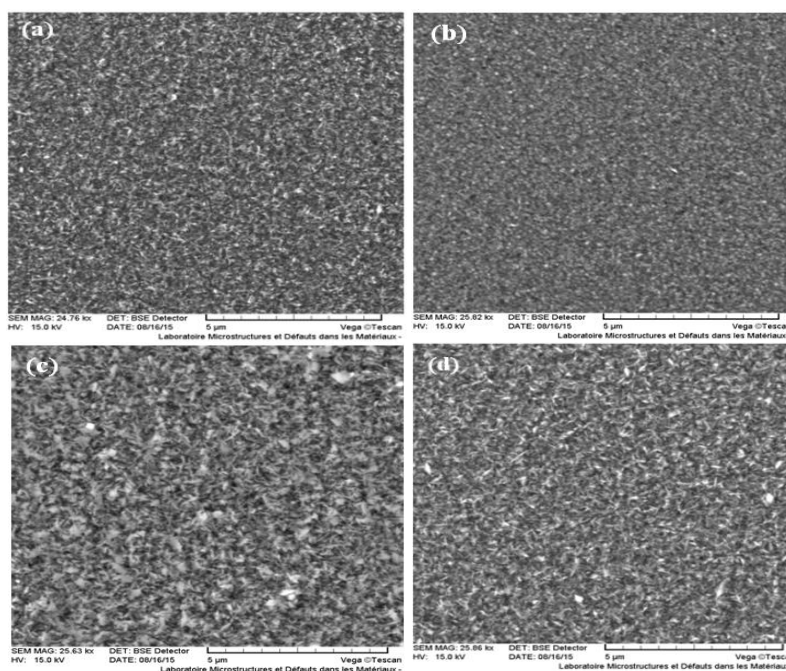


Fig.6. SEM image of 0-5 wt. % La doped ZnO thin films: a) undoped ZnO thin films, b) 1wt. %, c) 3wt. % and d) 5wt. %.

### 3.3. Removal of copper ions

Before starting the removal of copper ions, a calibration of different synthetic solutions current was proceed and curve of which is obtained by plotting the current of cathodic reduction peaks of cyclic voltammograms (CVs) versus fixed standard concentrations of copper chloride. Fig.7 displays cathodic voltammograms of copper solutions in concentrations range of  $3.15 \times 10^{-4}$  to  $15.8 \times 10^{-4}$  g/mL. CVs of the copper solutions were recorded between -1.2 and -0.0V/SCE at a scan rate  $50 \text{ mV} \cdot \text{s}^{-1}$ . All CVs exhibit peaks of reduction reactions at a potential range (-0.34 to -0.50V/SCE) which is due to the reduction of  $\text{Cu}^{+2}$  ions to Cu metal on the graphite carbon electrode; the cathodic peak current densities increase with the increase copper concentrations and exhibit a shift toward more negative potential. The calibration curve of the reduction current, versus the standard concentrations of copper, is shown in Fig.8.

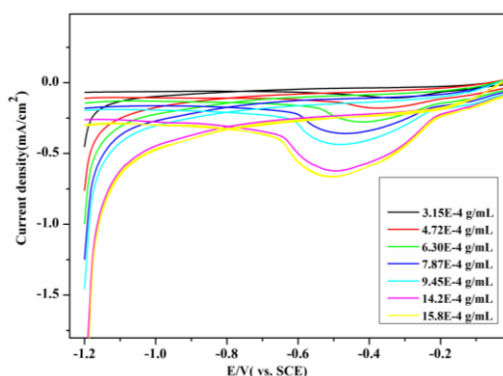


Fig.7. Cyclic voltammograms recorded for calibration curve with different copper concentrations, in the potential range -1.2 to -0.0 V versus SCE at  $50 \text{ mV}/\text{scan rate}$ .

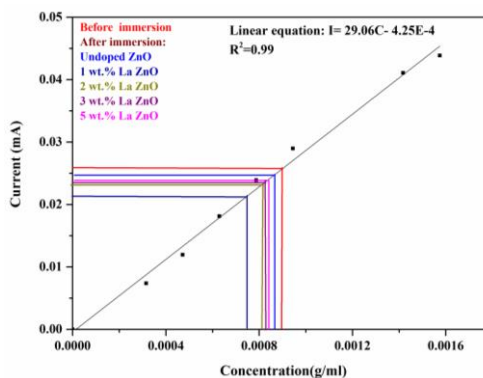


Fig. 8. Calibration curve of reduction current of  $\text{Cu}^{2+}$  versus standard concentrations of copper and reduction currents of residual solutions upon 0-5wt.% La doped ZnO immersed sheets in  $1.2 \cdot 10^{-2} \text{ M}$   $\text{CuCl}_2$  for 60min.

In order to determine the residual unknown concentration of copper in solution after each sheet immersion, CV was also preceded and recorded in the potential range -1.2 to 0.8V/SCE at a scan rate  $50 \text{ mV} \cdot \text{s}^{-1}$ . Fig. 9 shows the recorded CVs before and after each immersion. As can be seen three anodic peaks  $A_1$ ,  $A_2$  and  $A_3$  were observed approximately at potential -0.20V, 0.29V, and 0.58V/SCE. Peak  $A_1$  may be due to the stripping of copper metal from the electrode, peak  $A_2$  was assigned to the oxidation of Cu to  $\text{Cu}^{+1}$  ( $\text{Cu} \rightarrow \text{Cu}^{+1} + \text{e}^-$ ) and finely peak  $A_3$  was ascribed to the dissolution of copper metal leading to  $\text{Cu}^{+2}$  ions ( $\text{Cu} \rightarrow \text{Cu}^{+2} + 2\text{e}^-$ ). Two cathodic peaks  $C_1$ , and  $C_2$  were observed at potential -0.10V/SCE and at the potential plate (-0.50V to -0.43V/SCE) as seen in Fig. 9. Peak  $C_1$  is due to the reduction of  $\text{Cu}^{+2}$  ions to  $\text{Cu}^{+1}$  ( $\text{Cu}^{+2} + \text{e}^- \rightarrow \text{Cu}^{+1}$ ) and peak  $C_2$  is due to the reduction of  $\text{Cu}^{+2}$  ions to Cu metal on the graphite carbon electrode ( $\text{Cu}^{+2} + 2\text{e}^- \rightarrow \text{Cu}$ ); As

see from the inset of Fig. 9 that the cathodic peak  $C_2$  current densities decrease after having introduced undoped and La-doped ZnO samples, and the cathodic peak  $C_2$  slightly shifts to more positive potential. The current of the initial  $Cu^{2+}$  ions in asolution containing  $8.95 \times 10^{-4}$  g/mL of  $CuCl_2$  is 0.025mA before immersion and decreases until 0.021 mA after having immersed 1wt% La doped sample for 60 min. Currents values, before and immersion, are listed in Table3. Residual concentrations of  $Cu^{+2}$  ions (it means  $CuCl_2$ ), in solution, were obtained by intercepting its current to the concentration axis in g/mL via the calibration curve as plotted in Fig. 8.

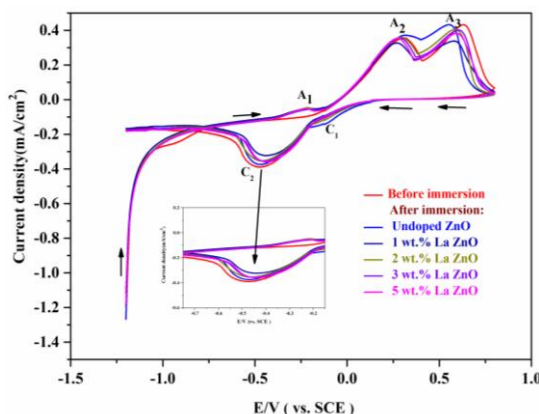


Fig.9. Cyclic voltammograms recorded, in  $1.2 \times 10^{-2} M$   $CuCl_2$  electrolyte in potential range -1.2 to 0.8V versus SCE and scan rate of 50 mV/s, for 0-5wt.% La doped ZnO sheets before and after each 60min of immersion.

Table 3. Measured currents, concentrations and removal percentages of copper  $Cu^{+2}$  ions from aqueous solution with La level doped ZnO.

Samples	Current(mA)	Concentration( $10^{-4}$ g/mL)	Percentage removal (%)
Before immersing sheets			
	0.02572	8.9586	//
After immersing sheets in ( $8.9586 \times 10^{-4}$ g/mL ) in copper solution for 60 min			
0wt.% La ZnO	0.02471	8.6275	3.69%
1wt.% La ZnO	0.02128	7.4535	16.80%
2wt.% La ZnO	0.02337	8.1383	9.15%
3wt.% La ZnO	0.02351	8.2851	7.51%
5wt.% La ZnO	0.02376	8.3829	6.42%

Percentage removal of copper as a histogram and the crystallite size are drawn in Fig. 10. Based on removal equation of  $Cu^{+2}$  ions and its associated histogram, it becomes clear that, in general, adsorption of copper on sheets (or removal efficiency) of La-doped ZnO thin films has higher removal than undoped ZnO. The removal efficiency of ZnO increases from 3.69% to 16.80% after La doping exhibiting the higher percentage removal of copper ions at 1wt.% La doping than undoped and the others La-doped ZnO thin films. Beyond 1wt. % La doping, removal of copper ions decreases to arrive at the minimum value of about 6.42% with 5wt.% La doping level. Removal values were illustrated in Table 3. Correlating the adsorption results with the crystallite size corresponding to 1wt.% La doped ZnO, it reveals that a link, between the removal and the surface area of samples, exists: the smallest grain size, as it was revealed in XRD study, provides great surface area (*i.e* decrease in grain size leads to sensitive nanostructure on the surface), yielding to more  $Cu^{+2}$  adsorption on the surface of the samples. This behavior may be credited to the presence of more active adsorption sites on the La-doped ZnO thin film surface [29] or also to the substitution of  $Zn^{+2}$  cation by  $La^{+3}$  hence 5 wt.% La doped sample has big crystallite size compared to the undoped one but it exhibits more  $Cu^{+2}$  removal, as seen in Fig. 10. This

further removal may be attributed to the increase in the permanent dipole toward  $c$  direction in the ZnO matrix attracting  $\text{Cu}^{+2}$  from the solution.

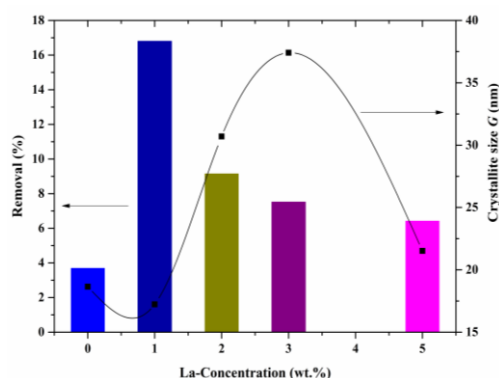


Fig.10. Drawn of a histogram with the cristalite size of La doped ZnO on the removal (adsorption) of  $\text{Cu}^{+2}$  ions from aqueous solution.

Both of the tow conceptions improving the removal of  $\text{Cu}^{+2}$  ions may be explained as follow:

The first one is the effect of the littleness in grain size mainly at lower level of doping (0-3 wt. % La) where the removal follows the decrease in grain size as seen in Fig. 10. As it is well known that the ZnO is polare material along  $c$  direction; the second conception is the effect of La doping in intensifying the permanent dipole along  $c$  direction. At 5 wt. % La doping, it is very importante to mentione that even tough the grain size increases, the removal increases too. This means that the insertion of La in Zn site increases the permanent dipole toward the  $c$  direction as shown in Fig. 11. The insertion is confirmed by XRD studies (see inset of Fig. 4) where the shift of the peak towards the lower angles is more significant in the case 5wt.% la doped sample. The permanent dipole intensification may be understood as follow: the insertion of La in ZnO matrix augmentains the lattice parameter ( $\hat{c} = c + \Delta c$ ) and the local ionic charge yielding to an augmentation in the local permanent dipole ( $\mu + \Delta\mu$ ) as illustrated in Fig. 11; the augmentation in the local permanent dipole lets the sample surface more attractive (adsorbitive) toward  $\text{Cu}^{+2}$ . As results, the adsorptive ability of thin films increases after La doping. Those results are in good agreement with similar results reported in the literature [13, 29, 30] which were obtained with Silver, Lanthanum and Gallium doped ZnO. More over, at nuked eye, one can observe that the layer of adsorped copper ions on the ZnO layer has the blue color of  $\text{Cu}^{+2}$  ion. Also after annealing the adsorped layer becomes black onwing the copper oxide color as exhibisited in Fig.12.

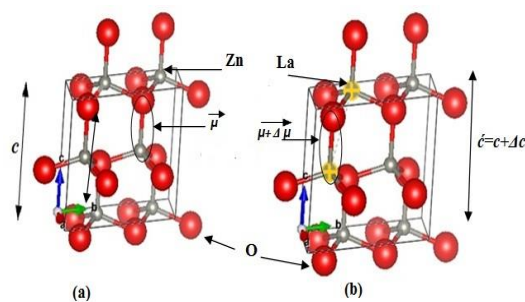


Fig.11. Effect of La in intensifaying the permanent dipole toward the  $c$  direction:  
a)  $\mu$  before doping, b)  $(\mu + \Delta\mu)$  after doping.

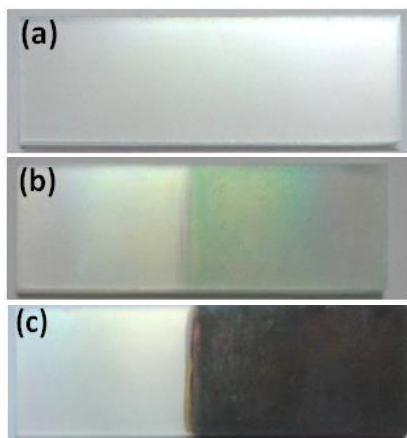


Fig.12. Photograph of La doped ZnO /glass slide: a) La doped ZnO before immersion, b) La doped ZnO after adsorption of copper ions and c) La doped ZnO / glass slide coated with CuO/Cu<sub>2</sub>O after annealing temperature (370° C).

#### 4. Conclusions

0-5wt.% La-doped zinc oxide thin films were deposited on 375°C heated glass by spray pyrolysis with moving nozzle. From UV-Visible transmission techniques, it was shown that the transmittance of the whole samples, was more than 75% in the visible region, and become more transparent after La doping. The Optical gap range was in 3.26-3.28eV. XRD studies show that thin films are a hexagonal wurtzite structure with (002) as preferred orientation whereas the crystalline size for all samples were averaged in 17-37nm. Use of the moving nozzle in providing homogenous distribution of ZnO product on the substrates was recognized by SEM images.

An enhancement in removal exceeding 16% of ion copper from the synthetic solution was achieved after 1wt. % La doping. For possible use in wastewater treatment, La is a good quality doping element for increasing the adsorptive ability of ZnO thin films by augmenting its active surface area or by intensifying the permanent polarity along *c* direction.

#### Acknowledgments

This work was supported in part by El-Oued University for measuring UV-Visible data. X-ray diffraction data in this work were acquired with an instrument supported by the University of Biskra. We thank also Chahra BOUKAOUS (Laboratoire Microstructures et Défauts dans les matériaux Univ-Constantine) for her assistance in SEM data acquisition.

#### References

- [1] C. Klingshirn, R. Hauschild, H. Priller, M. Decker, J. Zeller, H. Kalt, *Superlattices Microstruct***38**, 209(2005).
- [2] M. Mihailovic, A.-L.Henneghien, S. Faure, P. Disseix, J. Leymarie, A. Vasson, D. Buell, F. Semond, C. Morhain, J.Z. Pérez, *Optical Materials***31**, 532 (2009).
- [3] Z. Chunying, W. Jing, Z. Cheng, *Journal of Semiconductors***33**,072001 (2012).
- [4] Z. Huafu, L. Hanfa, L. Chengxin, Z. Aiping, Y. Changkun, *Journal of Semiconductors***31**, 083005 (2010).
- [5] Z.-X. Xu, V. Roy, P. Stallinga, M. Muccini, S. Toffanin, H.-F.Xiang, C.-M.Che, *Applied Physics Letters***90**, 223509 (2007).
- [6] S. Anandan, A. Vinu, T. Mori, N. Gokulakrishnan, P. Srinivasu, V. Murugesan, K. Ariga, *Catalysis Communications***8**, 1377 (2007).
- [7] V. Galstyan, E. Comini, C. Baratto, G. Faglia, G. Sberveglieri, *Ceramics International* **41**, 14239 (2015).

- [8] C. Boukaous, B. Benhaoua, A. Telia, S. Ghanem, *Materials Research Express* **4**, 105024 (2017).
- [9] Z. Sofiani, B. Derkowska, P. Dalasiński, M. Wojdyła, S. Dabos-Seignon, M.A. Lamrani, L. Dghoughi, W. Bała, Ó. Addou, B. Sahraoui, *Optics Communications* **267**, 433 (2006).
- [10] E. Elangovan, K. Ramamurthi, *J. Optoelectron. Adv. M.* **5**, 45 (2003).
- [11] P. Korake, R. Dhabbe, A. Kadam, Y. Gaikwad, K. Garadkar, *Journal of Photochemistry and Photobiology B: Biology* **130**, 11 (2014).
- [12] C. Mrabet, O. Kamoun, A. Boukhachem, M. Amlouk, T. Manoubi, *Journal of Alloys and Compounds* **648**, 826 (2015).
- [13] S. Azizian, M. Bagheri, *Journal of Molecular Liquids* **196**, 198 (2014).
- [14] M. Bagheri, S. Azizian, B. Jaleh, A. Chehregani, *Journal of Industrial and Engineering Chemistry* **20**, 2439 (2014).
- [15] M. Hua, S. Zhang, B. Pan, W. Zhang, L. Lv, Q. Zhang, *Journal of Hazardous Materials* **211**, 317 (2012).
- [16] J. Chen, J. Wang, F. Zhang, G. Zhang, Z. Wu, P. Yan, *Journal of Crystal Growth* **310**, 2627 (2008).
- [17] J. Tauc, R. Grigorovici, A. Vancu, *Physica Status Solidi (b)* **15**, 627 (1966).
- [18] F. Urbach, *Physical Review* **92**, 1324 (1953).
- [19] E. Burstein, *Physical Review* **93**, 632 (1954).
- [20] B. Benhaoua, A. Rahal, S. Benramache, *Superlattices and Microstructures* **68**, 38 (2014).
- [21] H.F. McMurdie, M.C. Morris, E.H. Evans, B. Paretzkin, W. Wong-Ng, L. Ettliger and C.R. Hubbard, *Powder Diffraction* **1**, 64 (1986).
- [22] J. Lu, Z. Ye, J. Huang, L. Wang, B. Zhao, *Applied Surface Science* **207**, 295 (2003).
- [23] M. Wang, W. Liang, Y. Yang, J. Yang, X. Cheng, S.H. Hahn, E.J. Kim, *Materials Chemistry and Physics* **134**, 845-850 (2012).
- [24] L. Xu, X. Li, Y. Chen, F. Xu, *Applied Surface Science* **257**, 4031 (2011).
- [25] P. Scherrer, *Gottin Nachricht* **2**, 98 (1918).
- [26] J.H. Wakelin, H.S. Virgin, E. Crystal, *Journal of Applied Physics* **30**, 1654 (1959).
- [27] S. Benramache, B. Benhaoua, H. Bentrach, *Journal of Nanostructure in Chemistry* **3**, 1 (2013).
- [28] Y. Bouznit, Y. Beggah, F. Ynineb, *Applied Surface Science* **258**, 2967 (2012).
- [29] T. Wu, Y. Ni, X. Ma, J. Hong, *Materials Research Bulletin* **48**, 4754 (2013).
- [30] I. Ghiloufi, J. El Ghoul, A. Modwi, L. El Mir, *Materials Science in Semiconductor Processing* **42**, 102 (2016).